

Enhancement of elliptic flow can signal a first order phase transition in high energy heavy ion collisions

Yasushi Nara,^{1,2} Harri Niemi,³ Akira Ohnishi,⁴ Jan Steinheimer,² Xiaofeng Luo,⁵ and Horst Stöcker^{2,3,6}

¹ Akita International University, Yuwa, Akita-city 010-1292, Japan

² Frankfurt Institute for Advanced Studies, D-60438 Frankfurt am Main, Germany

³ Institut für Theoretische Physik, Johann Wolfgang Goethe Universität, D-60438 Frankfurt am Main, Germany

⁴ Yukawa Institute for Theoretical Physics, Kyoto University, Kyoto 606-8502, Japan

⁵ Key Laboratory of Quark&Lepton Physics (MOE) and Institute of Particle Physics, Central China Normal University, Wuhan 430079, China

⁶ GSI Helmholtzzentrum für Schwerionenforschung GmbH, D-64291 Darmstadt, Germany

(Dated: August 21, 2017)

The beam energy dependence of the elliptic flow, v_2 , is studied in mid-central Au+Au collisions in the energy range of $3 \leq \sqrt{s_{NN}} \leq 30$ GeV within the microscopic transport model JAM. The results of three different modes of JAM are compared; cascade-, hadronic mean field-, and a new mode with modified equations of state, with a first order phase transition and with a crossover transition. The standard hadronic mean field suppresses the elliptic flow v_2 , while the inclusion of the effects of a first order phase transition (and also of a crossover transition) does enhance the elliptic flow at $\sqrt{s_{NN}} < 30$ GeV. This is due to the high sensitivity of v_2 on the early, compression stage, pressure gradients of the systems created in high energy heavy-ion collisions. The enhancement or suppression of the scaled energy flow, dubbed “elliptic flow”, $v_2 = \langle (p_x^2 - p_y^2)/p_T^2 \rangle$, is understood as being due to out of plane- flow, $p_y > p_x$, i.e. $v_2 < 0$, dubbed out of plane - “squeeze-out”, which occurs predominantly in the early, compression stage. Subsequently, the in-plane flow dominates, $p_x > p_y$, in the expansion stage, $v_2 > 0$. The directed flow, $v_1(y) = \langle p_x(y)/p_T(y) \rangle$, dubbed “bounce-off”, is an independent measure of the pressure, which quickly builds up the transverse momentum transfer in the reaction plane. When the spectator matter leaves the participant fireball region, where the highest compression occurs, a hard expansion leads to larger v_2 . A combined analysis of the three transverse flow coefficients, radial $v_0 \sim v_{\perp}$ -, directed v_1 - and elliptic v_2 - flow, in the beam energy range of $3 \leq \sqrt{s_{NN}} \leq 10$ GeV, distinguishes the different compression and expansion scenarios: a characteristic dependence on the early stage equation of state is observed. The enhancement of both the elliptic and the transverse radial flow and the simultaneous collapse of the directed flow of nucleons offers a clear signature if a first order phase transition is realized at the highest baryon densities created in high energy heavy-ion collisions.

PACS numbers: 25.75.-q, 25.75.Ld, 25.75.Nq, 21.65.+f

I. INTRODUCTION

The determination of the QCD equation of state (EoS) is one of the most important goals of high energy heavy-ion physics. For this purpose, the asymmetry of collective transverse flow in non-central nucleus-nucleus collisions, reflected in the directed flow $v_1 = \langle \cos \phi \rangle$ and elliptic flow $v_2 = \langle \cos 2\phi \rangle$ (where ϕ denotes the azimuthal angle of an outgoing particle with respect to the reaction plane, and angular brackets denote an average over particles and events), has been extensively studied. In hydrodynamics, the final state momentum space asymmetry reflects the pressure gradients in the early stage of the system and is therefore sensitive to the EoS [1–6]. A (first-order) phase transition generally exhibits a softest point, i.e. a minimum in the speed of sound, which is expected to have significant impact on the flow observables [7, 8]. Indeed, a local minimum of the directed flow [9–11] with a negative rapidity-slope of directed nucleon flow [10, 12–14] has been predicted by hydrodynamical simulations in the case of first-order phase transition. Recently, a negative rapidity slope of the proton directed flow has been observed in the BES program by the STAR Collaboration [15–17]. Although, a deeper understanding of the dynamics of directed flow has been achieved by recent more refined theoretical approaches [18–23], a consistent theoretical interpre-

tation of the experimental data on the excitation function of the directed flow has not been obtained yet.

The elliptic flow v_2 has been measured by various experiments from low to highest energies, currently available at LHC. At low energies, from several hundred AMeV up to $\sqrt{s_{NN}} = 4.3$ GeV, a negative elliptic flow of protons, with respect to the reaction plane, has been found [24–28] which is called the ‘squeeze-out’ [4]. This predominant out-of-plane flow is due to the presence of spectator matter, which blocks the participant particles escaping from the collision zone [5, 29]. Therefore, a higher pressure due to a hard EoS leads to a larger negative v_2 [30]. See Ref. [31] for a recent investigation on the detailed mechanism of the squeeze-out effect. This squeeze-out can be reproduced by transport models which include nuclear mean field, while cascade models cannot describe this effect. This indicates that the kinetic pressure from ideal resonance gas alone is too small. This lack of dynamical flow in the cascade type models have been recognized for directed flow as well [32, 33]. According to transport theoretical analysis in Ref. [5, 25, 29], the flow data up to top AGS energy $\sqrt{s_{NN}} < 5$ GeV can be described by repulsive mean field interactions at high density with the range of nuclear incompressibility of $K = 220 - 380$ MeV.

On the other hand, at higher incident energies, where the passing time of the spectators, t_{pass} , becomes shorter, and the

blocking effect of spectators becomes negligible, the expansion of participant matter is stronger towards the in-plane direction. Thus, the strength of v_2 is mainly determined by the initial transverse overlap geometry (spatial eccentricity) and the strength of the pressure gradient [36]. The passage time can be estimated by $t_{\text{pass}} = 2R/\gamma v$, where R is the radius of the nucleus, γ and v are the Lorentz factor and the incident velocity of the colliding nuclei, respectively. We expect the squeeze-out effect to become negligible above $\sqrt{s_{NN}} \approx 30$ GeV, since the passage time becomes less than 1 fm/c. Thus, at highest energies, the higher pressure leads to a stronger positive flow v_2 , in contrast to the beam-energy where the highest net-baryon densities are achieved in heavy-ion collisions. At RHIC and LHC, large elliptic flow values are found [37–41], which reach values compatible with ideal hydrodynamical predictions, i.e. with very small viscosities [42–46]. For recent reviews, see [47–52].

This paper discusses the collective flow in the beam energy region of the highest net-baryon densities [53] between 5 and 20 GeV: Here an interesting situation emerges, as pointed out in Ref. [54]: The passage time of two Au nuclei is ~ 5 fm/c at $\sqrt{s_{NN}} = 5$ GeV and 1.25 fm/c at 20 GeV. Thus, in this beam energy region, both the initial squeeze-out effect (mostly during the compression stages of the reaction) and the in-plane emission at the expansion stages are important, and the interplay of them determines the final strength of the elliptic flow. Ref. [54] compared transport calculations with and without hadronic mean field at $\sqrt{s_{NN}} = 5$ GeV. This work demonstrated that the final elliptic flow at mid-rapidity is very sensitive to the pressure at maximum compression, and it is conjectured that the analysis of the elliptic flow can constrain the EoS in dense matter.

The beam energy dependence of elliptic flow has been studied lately in distinctly different models [56–61]: The PHSD model predicts a smooth growth of the elliptic flow with the beam energy as a result of increasing importance of partonic degrees of freedom [55]. This seems consistent with recent measurements by the STAR collaboration [62]. The UrQMD hybrid model [56] finds that the contribution of the hydrodynamical stage to v_2 is small at $\sqrt{s_{NN}} = 5 - 7.7$ GeV. Other UrQMD hybrid model approach, with viscous hydrodynamics, reported that double the shear viscosity coefficient over entropy density ratio, η/s , is required to fit the elliptic flow at $7.7 < \sqrt{s_{NN}} < 11.5$ GeV as compared to the higher beam energies $\sqrt{s_{NN}} > 39$ GeV [59]. A three-fluid dynamical (3FD) model simulation shows low sensitivity of v_2 for charged hadrons to the EoS [61].

An important finding of the aforementioned model simulations is the strong dependence of the final elliptic flow on the treatment of the different stages of the collisions. In most of the so-called hybrid models, the different stages of the collisions are described by different approaches, e.g. transport theory first, then hydro, then again transport theories as after burner. These particular prescriptions and the various matching of the stages has substantial influence on the final observed elliptic flow. Such a complicated treatment was deemed necessary because most of the available standard hadronic transport models seemed to be unable to describe the large values

of the elliptic flow experimentally observed at the top RHIC and LHC energies. The general paradigm has become that this insufficient description of the v_2 values is due to a lack of interactions in the dense phase, missing multi particle interactions, as well as a lack of interactions between the pre-hadronic matter consisting of unformed hadrons.

On the other hand, such shortcomings are considered to be less important at beam energies which yield the highest net-baryon densities, from $\sqrt{s_{NN}} = 3 - 30$ GeV. This opens the opportunity to study super dense quarkyonic and baryonic matter via measurements of the elliptic flow in the beam energy range between 3 and 30 GeV, as we will demonstrate with the microscopic transport model JAM [63]: This single, consistent approach, used here does not require any sort of matching of different phases. JAM has significantly reduced systematic uncertainties studying the equation of state dependence of the elliptic flow in the highest net-baryon densities. The collective flows in mid-central Au+Au collisions are calculated in three different scenarios within JAM: a) the standard cascade mode [63], b) the standard hadronic mean field mode [64], and c) the cascade mode with a modified EoS [22, 23]. These three modes of the JAM simulations show different sensitivities of the three transverse collective flow valuables, the radial, the directed and the elliptic flow, on the EoS, within a single consistent transport approach.

This paper is organized as follows: Sec. II describes the salient features of the JAM transport approach. Sec. III presents the results for the excitation function of the elliptic flow. A detailed analysis of the collision dynamics is given in Sec. III C, which demonstrates the importance of a combined analysis of radial, directed, and elliptic flow. The conclusions are given in Sec. IV.

II. THE JAM MODEL

JAM [63] is a non-equilibrium microscopic transport model based on the resonance and string degrees of freedom. In JAM, particle production is modeled by the excitation and decay of resonances and strings as employed by other models [65–67]. Secondary products from decays of resonances or strings can interact with each other via binary collisions which generate collective flows. A detailed description of the hadronic cross sections and cascade method implemented in the JAM model can be found in Ref. [63, 68]. In addition to the standard cascade simulation, the hadronic mean field interaction has been incorporated in JAM [64, 69] based on the simplified version of relativistic molecular dynamics (RQMD/S) [70, 71]. The RQMD approach [72] is formulated to describe the covariant dynamics of N interacting particle system based on the constrained Hamiltonian dynamics, in which Hamiltonian is constructed from the sum of constraints, and the equations of motion are obtained by the condition that the constraints must be conserved during the time evolution. The RQMD/S formulation uses the same mass shell conditions as the original RQMD formulation. The difference is the choice of the simplified time fixation constraints which fix the time of the particles. The time fixations are chosen so that

TABLE I: Parameter set of the potentials in the mean field mode which yields the incompressibility of $K = 270, 370$ MeV in momentum-dependent soft (MS) and hard (MH), respectively. $\rho_0 = 0.168 \text{ 1/fm}^3$ is used for the normal nuclear matter density.

type	K (MeV)	α (GeV)	β (GeV)	γ	μ_1 (1/fm)	μ_2 (1/fm)	C_1 (GeV)	C_2 (GeV)
MS	270	-0.209	0.284	7/6	2.02	1.0	-0.383	0.337
MH	370	-0.0122	0.0874	5/3	2.02	1.0	-0.383	0.337

the time of all the particles are set to be the same in a reference frame. If we further assume that the mean field is smaller than the kinetic energy of the particles, which is justified in high energy collisions, thus replacing the p_i^0 component as the kinetic energy in the argument of the potentials, one can solve for the Lagrange multipliers analytically. As a result, the formulation is equivalent to the Hamiltonian system

$$H = \sum_{i=1}^N \sqrt{\mathbf{p}_i^2 + m_i^2 + 2m_i V_i} \quad (1)$$

with the equations of motion

$$\begin{aligned} \frac{d\mathbf{r}_i}{dt} &= \frac{\partial H}{\partial \mathbf{p}_i} = \frac{\mathbf{p}_i}{p_i^0} + \sum_{j=1}^N \frac{m_j}{p_j^0} \frac{\partial V_j}{\partial \mathbf{p}_j}, \\ \frac{d\mathbf{p}_i}{dt} &= -\frac{\partial H}{\partial \mathbf{r}_i} = -\sum_{j=1}^N \frac{m_j}{p_j^0} \frac{\partial V_j}{\partial \mathbf{r}_j}. \end{aligned} \quad (2)$$

Thus, the numerical cost of our approach is the same as the non-relativistic quantum molecular dynamics simulations. RQMD/S approach has been successfully applied to the various reactions [64, 71, 73]. A similar approach is employed to describe the quark dynamics based on the NJL model [74]. We only consider a effect of hadronic mean field potentials in this work. The effects of both partonic and hadronic mean fields have been studied in the AMPT model [75].

In the RQMD/S approach, particles acquire an effective mass $m_i^* = \sqrt{m_i^2 + 2m_i V_i}$ as a result of the interaction with the other particles, where the scalar one-particle potential V_i is given by the sum of the Skyrme-type, density dependent terms and the Lorentzian-type, momentum dependent terms:

$$\begin{aligned} V_i &= \frac{\alpha}{2\rho_0} \langle \rho_i \rangle + \frac{\beta}{(1+\gamma)\rho_0^\gamma} \langle \rho_i \rangle^\gamma \\ &+ \sum_{k=1,2} \frac{C_k}{2\rho_0} \sum_{j(\neq i)} \frac{1}{1 + [p_{ij}/\mu_k]^2} \rho_{ij}. \end{aligned} \quad (3)$$

Here,

$$\langle \rho_i \rangle = \sum_{j(\neq i)} \rho_{ij} = \sum_{j(\neq i)} (4\pi L)^{-3/2} \exp(q_{ij}^2/4L) \quad (4)$$

and q_{ij}^2 and p_{ij}^2 are the relative distance and momentum squared between particles i and j in their center of mass frame. The Gaussian width is taken to be $L = 1.08 \text{ fm}^2$ [76].

Potential parameters are determined by fulfilling the nuclear saturation properties and the global optical potential [77]. In this paper, the parameter set listed in Table I is employed. The parameter set MS is used throughout this paper except for the results in Table II.

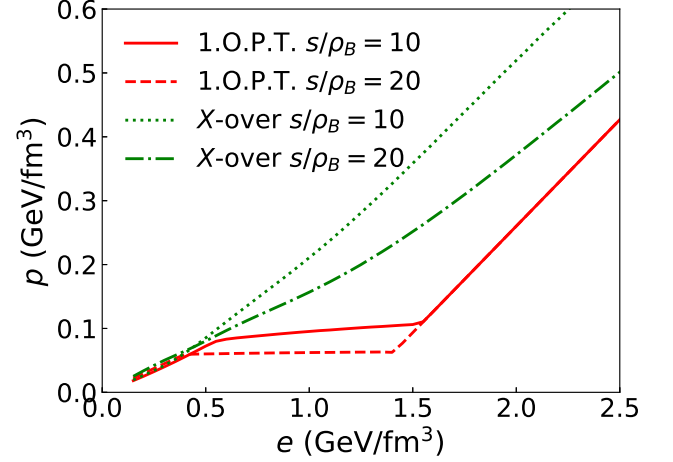


FIG. 1: EoS implemented in JAM. The solid and dashed lines represent the EoS with a first order phase transition for the ratio of entropy to baryon density $s/\rho_B = 10$ and 20 respectively, and the dotted and dotted-dash lines represents the EoS with a crossover for $s/\rho_B = 10, 20$.

We also study the effect of the EoS on the elliptic flow by employing the method proposed by Ref. [78] based on the virial theorem [79], in which the scattering style of the two-body collisions are modified so as to control the pressure of the system. In this method, the azimuthal angle of the two-body scattering between particle i and j is constrained by [23]

$$\Delta P = \frac{\rho}{3(\delta\tau_i + \delta\tau_j)} \Delta \mathbf{p}_{ij} \cdot \Delta \mathbf{r}_{ij}, \quad (5)$$

where ρ is the Lorentz invariant local particle density and $\delta\tau_i$ is the proper time interval between successive collisions. $\Delta \mathbf{p}_{ij}$ is the momentum transfer and $\Delta \mathbf{r}_{ij} = \mathbf{r}_i - \mathbf{r}_j$ is the relative coordinate between particle i and j in the two-body c.m. frame. ΔP is the deviation of the pressure from the ideal gas value. An advantage of this method is to provide a numerically efficient way to modify the EoS of a system according to a given EoS table. We implemented the effects of both the EoS with a first-order phase transition (JAM-1.O.P.T.) and a crossover transition (JAM-X-over) based on this method [23]. For the first-order phase transition EoS, we use the same model as the so-called EOS-Q [80]. For the crossover (X-over) EoS, we use the chiral model EoS from Ref. [81]. Here the EoS at vanishing baryon density is consistent with a smooth crossover transition, as found in lattice QCD. That EoS predicts two critical points at $\mu_B \approx 900$ and 1400 MeV. The EoS from both models, EOS-Q and X-over implemented in this work are compared in Fig. 1 for entropy to baryon density $s/\rho_B = 10$ and 20 .

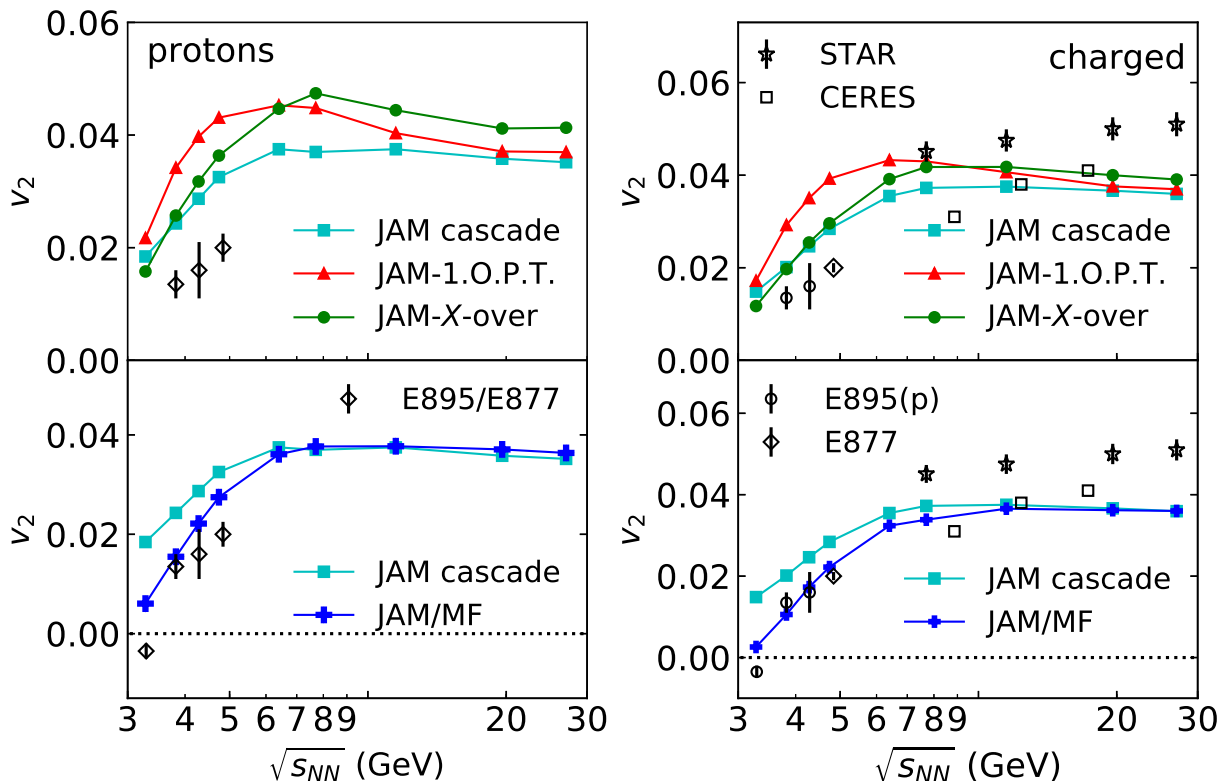


FIG. 2: Beam energy dependence of the elliptic flows v_2 of protons at $|y| < 0.2$ (left) and charged hadrons at $|\eta| < 0.2$ (right) in mid-central Au+Au collisions ($4.6 \leq b \leq 9.4$ fm) from JAM cascade mode (full squares), JAM with first-order EoS (full triangles), crossover EoS (full circles), and JAM with hadronic mean field (full crosses). Data are from the E895/E877 [25, 35], CERES [34], and STAR [62] collaborations.

III. RESULTS

In the following we will present computations of the elliptic flow in mid-central Au+Au collisions, and compare the hadronic mean field results with the two types of EoS described above. In the simulation, we choose the mid-impact parameter range $4.6 < b < 9.4$ fm, which is reasonable for mid-central collisions.

A. Elliptic flow excitation functions

Fig. 2 shows the beam energy dependence of the elliptic flow v_2 of protons at mid-rapidity $|y| < 0.2$, (left panel), and charged particles, ($|\eta| < 0.2$) (right panel), in mid-central Au+Au collisions using the standard JAM cascade mode, JAM with a first-order phase transition (JAM-1.O.P.T.), JAM with a crossover EoS (JAM- X -over) and JAM with hadronic mean field (JAM/MF), compared to data from the STAR, CERES, and E895/E877 collaborations [25, 34, 35, 62]. JAM in the cascade mode does not reproduce the v_2 -values in the measured beam energy region: The calculations overpredicts v_2 below $\sqrt{s_{NN}} = 5$ GeV, while it underpredicts v_2 above $\sqrt{s_{NN}} = 7.7$. At lower AGS energies, $\sqrt{s_{NN}} < 5$ GeV, the inclusion of nuclear mean fields reduces the v_2 values significantly, and the JAM/MF mode calculations are in reason-

able agreement with the data, consistent with previous work [5, 25, 29, 66]. Thus, high pressure in the early stages of heavy-ion collision achieves a stronger squeeze-out at low beam energies. Certain model uncertainties prevail related to the implementation of mean field: In the RQMD/S approach, potentials are included as Lorentz scalars. However, vector potential yield stronger repulsion effects than scalar potentials. In fact, the present model yields slightly larger v_2 values than seen in predictions by the BUU- [5, 25, 29] and UrQMD model [66], in which vector potentials are implemented. Influence of vector potentials on v_2 is checked by simulating the potential in Eq.(3) as the zeroth component of a vector potential [89]. It is found that v_2 is more suppressed, up to AGS energies (about a 20% reduction at $\sqrt{s_{NN}} = 4.74$ GeV), but that effect is small at higher energies.

In contrast, calculations with a soft EoS, such as JAM-1.O.P.T. and JAM- X -over, yield larger v_2 values, which lead to smaller early pressure gradients, resulting in less squeeze-out. All calculations lead to similar v_2 values at high energies. The calculated v_2 values here are lower than the data. This may indicate the need to include parton dynamics, as conjectured by PHSD simulations [55], where the dynamics of the partonic phase becomes relevant at beam energies above $\sqrt{s_{NN}} = 10$ GeV. Hybrid models predict comparable v_2 values, above $\sqrt{s_{NN}} = 10$ GeV [59], if a hydrodynamic phase with small viscosity is included in the simulation.

Our results suggest that the intermediate energy region,

$5 < \sqrt{s_{NN}} < 7.7$ GeV, is most interesting: If there is no softening of the EoS, and the hadronic pressure dominates, v_2 must be suppressed to nearly the same values as in the cascade calculations. On the other hand, if the softening of the EoS plays an important role, then v_2 -values are enhanced.

Strong initial non-equilibrium pressure due to the hadronic mean-field explains the suppression of the elliptic flow at AGS energies. The dynamical treatment of a first order chiral phase transition in a non-equilibrium real-time dynamics predicts strong reduction of elliptic flow [82].

B. Event-plane method and Cumulants

Various methods have been proposed to extract the anisotropic flows. As the reaction plane is not a priori known in heavy ion experiments, different methods on how to extract elliptic flow must be tested. First, elliptic flow $v_2\{\text{EP}\}$ is computed by the event-plane method [83], where the anisotropic flow coefficients $v_n\{\text{EP}\}$ are given by

$$v_n\{\text{EP}\} = \frac{\langle \cos[n(\phi - \Psi_n)] \rangle}{\sqrt{2} \langle \cos[n(\Psi_n^A - \Psi_n^B)] \rangle}. \quad (6)$$

The event plane angle Ψ_n is then estimated from the event flow vector Q_n via

$$\Psi_n = \arg(Q_n)/n, \quad Q_n = \sum_j w_j e^{in\phi_j}, \quad (7)$$

where the sum runs over all particles used in the event-plane determination except for the particle actually used for the evaluation of v_2 , to remove self-correlations. Here particles with $1 < |\eta| < 3$ are used to avoid self-correlations in the calculations of v_2 at mid-rapidity. ϕ_j is the azimuthal angle for the j -th particle in the momentum space. The transverse mass of particle i is used as the weight $w_j = m_{Tj}$. Two subevents, A and B , are used to estimate the event plane resolution in the denominator of Eq. (6). The two subevents are defined - in the forward (A : $-3 < \eta < -1$) and - in the backward (B : $1 < \eta < 3$) regions.

Another standard method is the cumulant method: here multi-particle correlations are used to extract the anisotropic flow parameters [84, 85]. The scalar product method [86] is used in order to suppress the so-called non-flow effects, by imposing pseudo-rapidity gap $|\Delta\eta|$. This method separates the particles in the mid-rapidity region into two subevents, a and b , each with multiplicity, M_a and M_b , which are separated by a rapidity gap. The formula[86, 87]

$$v_n\{2, |\Delta\eta|\} = \sqrt{\frac{\langle Q_n^a Q_n^{b*} \rangle}{\langle M_a M_b \rangle}} \quad (8)$$

now computes $Q_n^{a/b}$ from the particles in the two regions respectively, as separated by the gap $|\Delta\eta|$ in the event with the weight $w_j = 1$.

Fig. 3 compares elliptic flows of charged hadrons at mid-rapidity, $|\eta| < 0.5$, extracted by these different methods

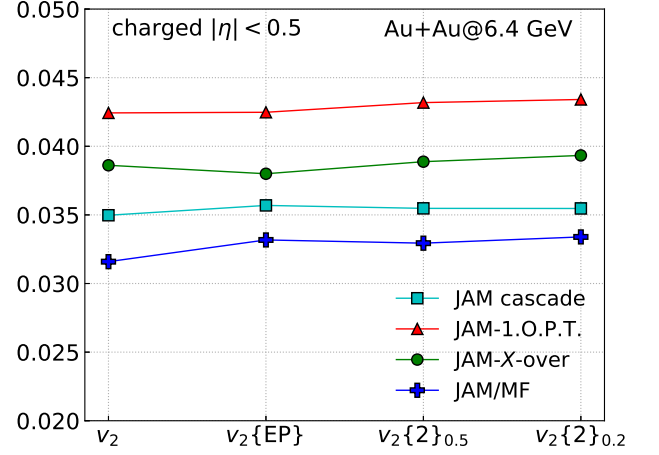


FIG. 3: Comparison of elliptic flow at mid-rapidity ($|\eta| < 0.5$) extracted by different methods in mid-central Au+Au collisions at $\sqrt{s_{NN}} = 6.4$ GeV for cascade mode (squares), first-order EoS (triangles), crossover EoS (circles), and hadronic mean field mode (crosses). $v_2\{2\}_{0.5}$ and $v_2\{2\}_{0.2}$ correspond to the results with pseudo-rapidity gaps of $|\Delta\eta| > 0.5$ and $|\Delta\eta| > 0.2$ respectively.

in mid-central Au+Au collisions at $\sqrt{s_{NN}} = 6.4$ GeV. Fig. 3 shows different values for the rapidity gap denoted by $v_2\{2\}_{0.5}$ and $v_2\{2\}_{0.2}$, corresponding to $|\Delta\eta| > 0.5$ and $|\Delta\eta| > 0.2$. Observe that both, event-plane and cumulant methods, are close to the reaction plane elliptic flow v_2 value for all modes in JAM. The results are similar for other beam energies. Hence, these conclusions are robust with respect to the different methods used to extract the elliptic flow. The STAR collaboration [62] reported that the difference between four-particle cumulants $v_2\{4\}$ and $v_2\{2\}$ reduces at the lower collision energies, and that $v_2\{4\} \approx v_2\{2\} \approx v_2\{\text{EP}\}$, for mid-central collisions at $\sqrt{s_{NN}} \leq 11.5$. Our results are consistent with these observations.

The next section examines in detail the collision dynamics, in particular how the elliptic flow is generated during the reaction.

C. Analysis of the collision dynamics

The sensitivity of the elliptic flow on the early pressure gradients, i.e. the EoS is analysed in Fig. 4, by examining the time evolution of the local isotropic pressure p , and the energy density e , averaged over events, in mid-central Au+Au collision at $\sqrt{s_{NN}} = 6.4$ GeV. The results are compared for the different EoS employed in JAM. These quantities are averaged values over collision points, thus those particles which have not yet collided are not included in the evaluation. We evaluate the non-ideal pressure by using Eq. (5), as in Ref. [23], for both the JAM-1.O.P.T. and the X -over mode. For the potential interactions in the JAM/MF mode, the pressure from the potential contribution ΔP_{pot} is given locally by [54]

$$\Delta P_{\text{pot}} = \frac{\rho}{3} (\mathbf{F}_i \cdot \mathbf{r}_i + \mathbf{F}_{ri} \cdot \mathbf{p}_i). \quad (9)$$

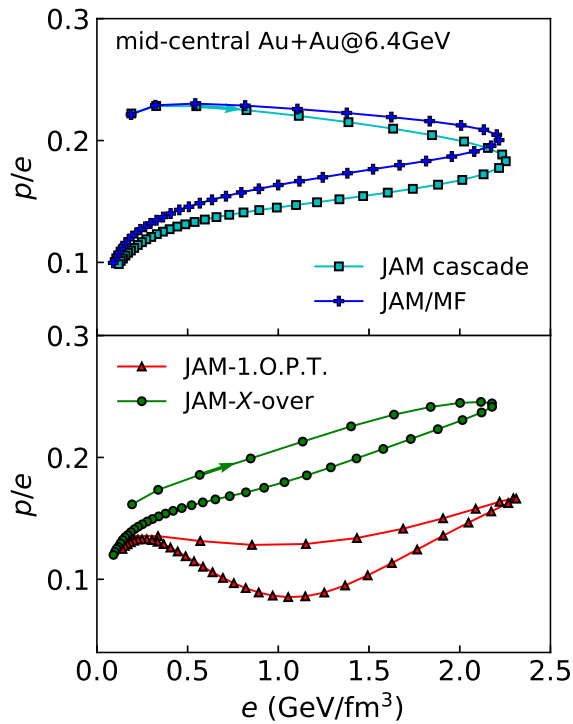


FIG. 4: Time evolution of the isotropic pressure p , and energy density e in mid-central Au+Au collisions at $\sqrt{s_{NN}} = 6.4$ GeV calculated in the JAM cascade mode (squares), first-order EoS (triangles), crossover EoS (circles), and hadronic mean field mode (crosses). Initial points correspond to the time 0.375 fm/c, after the touching of the two nuclei, and the time interval is 0.25 fm/c. Arrows indicate the direction of the time evolution of the reactions. Pressure and energy density are averaged over collision points in a cylindrical volume of transverse radius 3 fm and a longitudinal distance of 2 fm centered at the origin.

Here ρ is the particle density, F_i and F_{r_i} are the forces exerted on the i -th particle due to the density- and the momentum-dependent parts of the potentials, respectively. The JAM/MF-EoS is stiffer than the EoS in the cascade mode, due to the density- as well as momentum-dependent potentials which predict repulsive interactions at high baryon densities. The mean field effects are more pronounced at lower energies in JAM/MF. In stark contrast to the JAM/MF mode, the EoS with the first-order phase transition (JAM-1.O.P.T.) predicts very low p/e values, indicating a small sound velocity; while the crossover EoS is softer than that of the cascade mode, in the early stages of the collisions. Just this EoS becomes the stiffest EoS at the maximum overlap of the two nuclei. The origin of the hardness of the EoS is similar between JAM/MF and JAM-X-over: In JAM/MF, the EoS is hard because of the repulsive hadronic interactions, in the crossover EoS the dense hadronic part of the EoS is stiff due to hard core repulsion effects. Bag model massless ideal gases of quarks and gluons is used in the JAM-1.O.P.T.. Hence, the QGP phase has the same p and e dependence, independent of the baryon density. After the system expands and reaches the hadronic phase, all EoS are harder than the EoS in the JAM cascade mode, due to

the repulsive potentials implemented in the EoS.

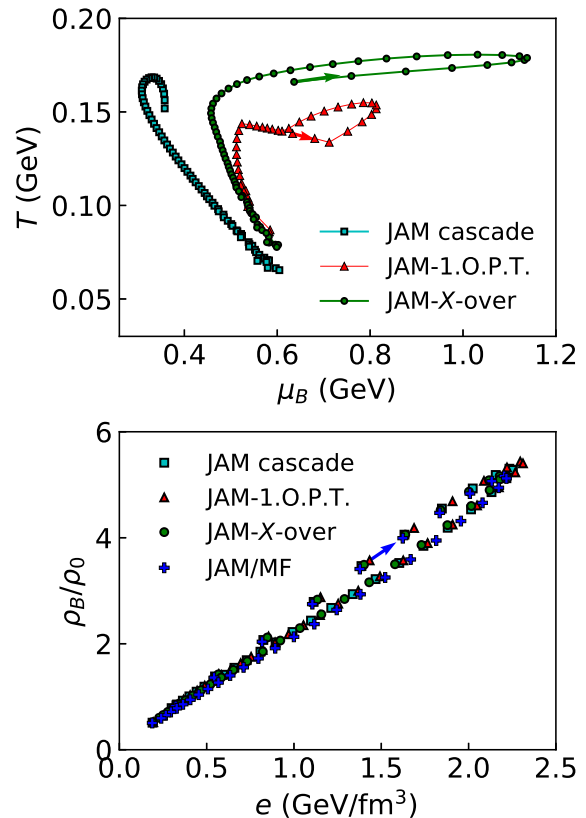


FIG. 5: Time evolution of temperature T and baryon chemical potential μ_B (upper panel), and net-baryon density ρ_B/ρ_0 , and energy density e (lower panel) in mid-central Au+Au collisions at $\sqrt{s_{NN}} = 6.4$ GeV.

Fig. 5 displays the time evolution of the temperature T , the baryon chemical potential μ_B , the net-baryon density ρ_B/ρ_0 , and the energy density e in mid-central Au+Au collision at $\sqrt{s_{NN}} = 6.4$ GeV. All modes yield similar behavior for both, the net-baryon density and the energy density. However, the T - μ_B evolutions are quite different among different EoS. Both, the first order phase transition and the crossover transition, are clearly seen by the trajectories in the T - μ_B plane. The crossover EoS in JAM follows similar trajectory as an isotropic expansion using the lattice QCD calculations [88].

Besides the uncertainty in the EoS, there is another model degree of freedom in the JAM EoS-modified mode, where the pressure is controlled by imposing a static equilibrium EoS $p(e, \rho_B)$. This prescription may be inadequate when the system is in a highly non-equilibrated state, as in particular, during the very early stages of the collisions. Keep this feature in mind for the analysis below. This problem does not exist in the mean field approach, which treats the effect of the EoS naturally in the non-equilibrium stages of the collisions.

The elliptic flow is sensitive to the initial deformation of the almond shape participant, geometry representing in non-central collisions: Fig. 6 shows the time evolution of the eccentricity ϵ of the system in Au+Au collision at $\sqrt{s_{NN}} = 6.4$

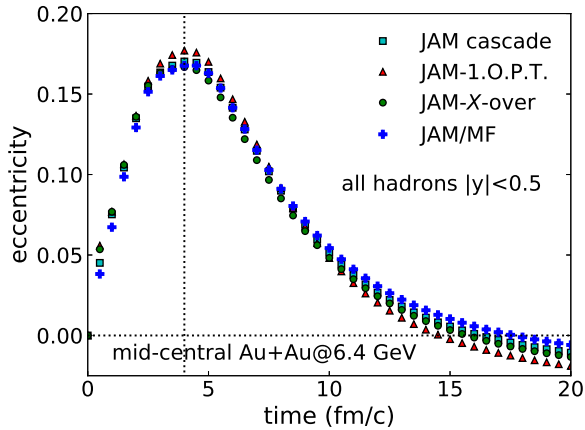


FIG. 6: The time evolution of the eccentricity ϵ as evaluated from all particles in mid-rapidity $|y| < 0.5$.

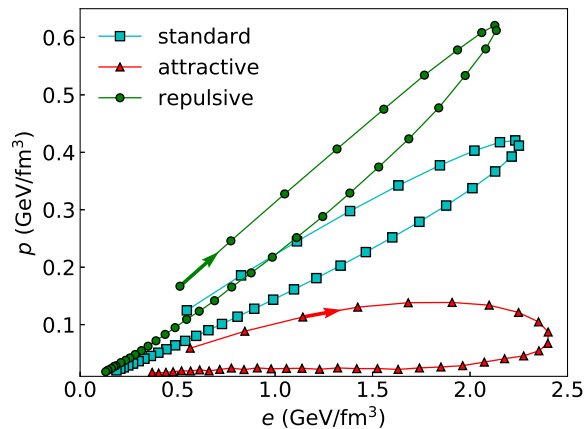


FIG. 7: Time evolution of the local pressure p and energy density e in mid-central Au+Au collision at $\sqrt{s_{NN}} = 6.4$ GeV for JAM standard cascade simulation (squares), JAM with attractive orbit (triangles), and JAM with repulsive orbit (circles).

GeV defined as

$$\epsilon = \left\langle \frac{y^2 - x^2}{x^2 + y^2} \right\rangle. \quad (10)$$

Note that the eccentricity of the system reaches a maximum at time $t = 4$ fm/c, the passage time of the spectators for this incident energy. Thus, the role of the pressure flips at this time, $t = 4$ fm/c: higher pressure leads to a reduction of v_2 at $t < 4$ fm/c, while higher pressure leads to an enhancement of v_2 at $t > 4$ fm/c. Observe that JAM-1.O.P.T. yields the largest eccentricity caused by the compression of the system. This large eccentricity generates large v_2 -values even though the JAM-1.O.P.T. mode gives the lowest pressure among the different modes.

The interplay between the initial pressure and late pressure, (initial and late pressure is defined as the pressure before or after the passage time t_{pass} of the spectators), is studied by performing simulations which impose either attractive or

pulsive orbits for all two-body collisions. Changing this “collision style” is known to change the pressure of the system. Selecting attractive orbits in a two-body scattering reduces the pressure. On the other hand, repulsive orbits enhance the pressure.

The time evolution of the effective EoS for each simulation is shown in Fig. 7. Note that the pressure is modified by an order of magnitude in these simulations. As expected, simulations with attractive orbits significantly soften the EoS, while, repulsive orbit simulations show extremely high pressure values. The time evolution of v_2 for these particular cases are shown in Fig. 8. The reduction of v_2 , due to initial high pressure in the repulsive orbit simulation, is partially canceled by the enhancement of the v_2 during the late expansion stages. Note that the same cancellation occurs in the attractive orbit simulation. In our previous work [22], attractive orbit simulations yielded the nearly the same v_2 -values as the JAM cascade mode for charged hadrons from $\sqrt{s_{NN}} = 7.7$ GeV up to $\sqrt{s_{NN}} = 27$ GeV. This is understood as being due to the cancellations on v_2 . On the other hand, attractive orbit simulations at lower incident energies, $\sqrt{s_{NN}} \leq 7$ GeV, yield an enhancement of v_2 , because the initial pressure dominates the final value of elliptic flow at such low beam energies [90].

The role of initial and final pressures is demonstrated in Fig. 8 by increasing the rate of two-body hadron-hadron collisions in the simulation: Here, the cascade simulation uses zero hadron formation time, to simulate faster equilibration with highest pressure by increasing the number of collision. Still, one notes the partial cancellation even in these calculations. Zero formation time simulations using UrQMD at $\sqrt{s_{NN}} = 200$ GeV reach the ideal hydro limit [91]. This cancellation may be the reason why 3FD model simulations show an insensitivity of v_2 to the EoS [61] at the STAR BES energies.

The compensating effects of early and late pressures are explicitly confirmed by a simulation in which attractive orbits are selected *before* the passage time $t_{\text{pass}} = 4$ fm/c, but repulsive orbits are selected *after* the passing of the spectator nucleons: Here, a strong enhancement of v_2 is expected, and, vice versa, v_2 should drop, if repulsive orbits are employed *before* t_{pass} , and attractive orbits *after* t_{pass} . Indeed, the predicted enhancement of v_2 as well as the reduction of v_2 are manifested in such simulations, see Fig. 8 (stars and crosses). This proves that the final values of the elliptic flow are due to the (partial) cancellation of the early squeeze-out with the subsequent in-plane bounce off flow [2]. This analysis allows to summarize the different stages of the collision dynamics leading to the different values of v_2 at beam energies below $\sqrt{s_{NN}} \approx 10$ GeV as follows:

- (i) For the hadronic mean field case, elliptic flow is suppressed-because the initial squeeze-out due to repulsive potentials is stronger than the late in-plane flow, for beam energies $\sqrt{s_{NN}} \lesssim 5.5$ GeV. At higher beam energies, elliptic flow is nearly the same in the MF case as in the cascade mode, due to cancellations and less effect of the potentials.
- (ii) For the first-order phase transition, the system is mostly

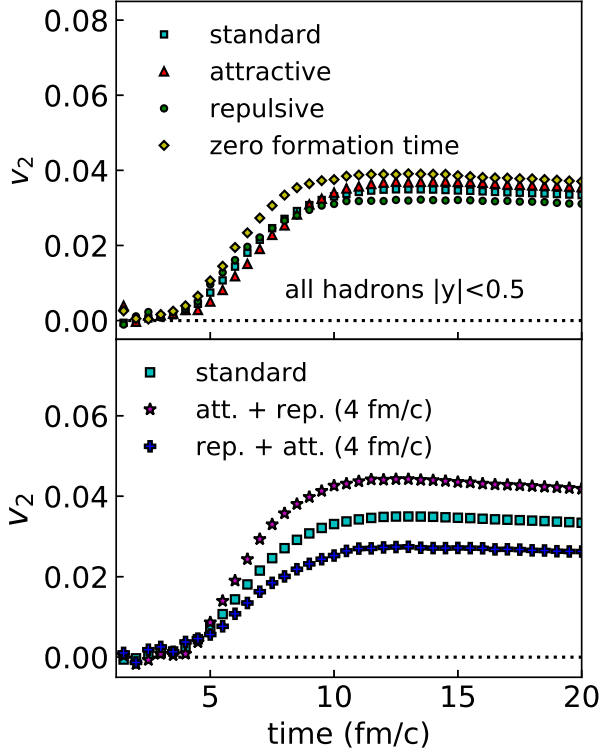


FIG. 8: Upper panel: The time evolution of v_2 in mid-central Au+Au collision at $\sqrt{s_{NN}} = 6.4$ GeV for JAM standard cascade simulation (squares), JAM with attractive orbit (triangles), and JAM with repulsive orbit (circles). Diamonds show the results from the JAM standard cascade mode with zero formation time. Lower panel: JAM with attractive (repulsive) orbit before the passing of spectators time $t < 4$ fm/c and repulsive (attractive) orbit at $t > 4$ fm/c are shown by stars (crosses).

inside of the soft region in this beam energy range, and the pressure is always very low. This leads to high compression and to a very soft expansion of the system. In addition, this softening generates large eccentricities. As a consequence, a first-order phase transition largely suppresses the initial squeeze-out. Hence, it yields large positive v_2 - even though the pressure is low.

- (iii) For the crossover transition, the pressure is soft in the initial compression stage, but it becomes high in the expansion stage. As a result, the final elliptic flow is large.

D. Radial, directed and elliptic flows

Turning to the combined analysis of the three different flow coefficients, namely the radial, directed and elliptic flow, distinction of different effects of the EoS on the different flow coefficients are observed. This independent sensitivities allow for distinguishing the different expansion dynamics.

Fig. 9 displays the time evolution of the average transverse mass $\langle m_T \rangle - m_0$, where $m_T = \sqrt{p_T^2 + m_0^2}$, the sign

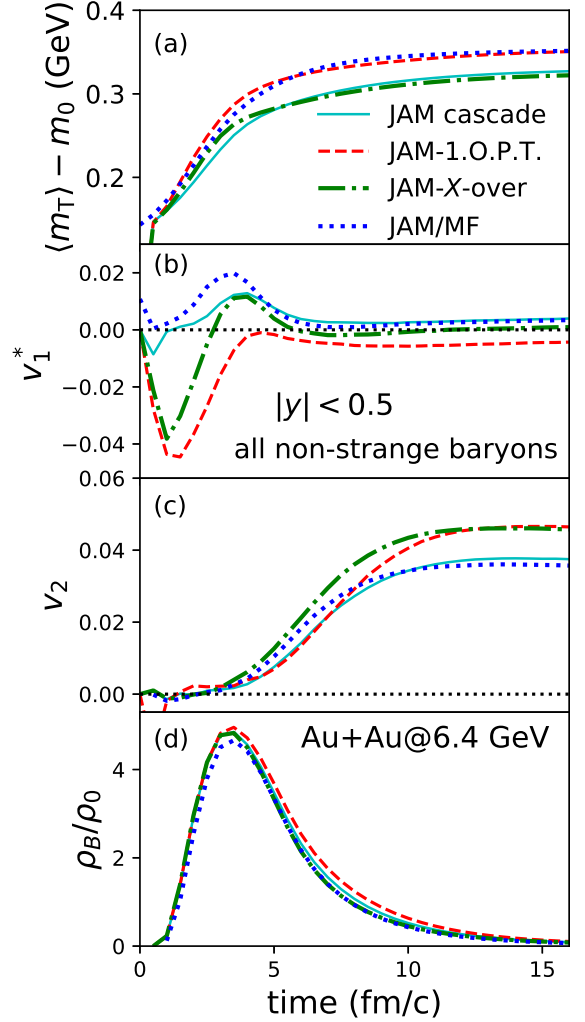


FIG. 9: The time evolution of (a) average transverse mass $\langle m_T \rangle - m_0$, (b) sign weighted directed flow v_1^* , (c) elliptic flow v_2 for baryons at mid-rapidity $|y| < 0.5$ in mid-central Au+Au collision at $\sqrt{s_{NN}} = 6.4$ GeV. Time evolution of normalized baryon density ρ_B/ρ_0 averaged over a cylindrical volume of transverse radius 3 fm and longitudinal distance of 1 fm is displayed in the panel (d). Solid, dashed, dashed-dotted, and dotted lines show the results from JAM cascade, JAM with first-order phase transition, JAM with crossover EoS, and JAM with hadronic mean field simulations, respectively.

weighted directed flow,

$$v_1^* = \int dy v_1(y) \text{sgn}(y), \quad (11)$$

and the elliptic flow v_2 , of baryons at mid-rapidity, $|y| < 0.5$, as well as the normalized net-baryon density, in Au+Au collision at $\sqrt{s_{NN}} = 6.4$ GeV for four different cases: Here, $\langle m_T \rangle - m_0$ characterizes the strength of the radial transverse flow. Both JAM-1.O.P.T. and JAM/MF simulations yield the enhanced $\langle m_T \rangle$. However, the dynamical origin of the large radial flow is different: The radial flow in JAM/MF is gener-

TABLE II: Slope parameter T_{eff} , the slope of directed flow dv_1/dy and the elliptic flow v_2 of mid-rapidity ($|y| < 0.2$) nucleons in mid-central Au+Au collision at $\sqrt{s_{NN}} = 6.4$ GeV. The comments in the parenthesis are relative to the cascade mode. Scalar type momentum dependent hard (MH/Scalar) and soft (MS/Scalar) mean field, and vector type momentum dependent hard (MH/Vector) and soft (MS/Vector) mean field are also compared.

	T_{eff} (MeV)	v_1 slope (%)	v_2 (%)
cascade	259	2.46	3.74
1st-order	278 (enhanced)	-0.34 (negative)	4.45 (enhanced)
crossover	257 (same)	1.52 (positive)	4.47 (enhanced)
MS/Scalar	271 (enhanced)	2.28 (positive)	3.61 (same)
MH/Scalar	274	2.33	3.54
MS/Vector	268	2.59	3.33
MH/Vector	270	3.08	3.23

ated due to the hadronic repulsive potentials, while in JAM-1.O.P.T. it is the result of the stronger compression of the system, and the longer lifetime of the system. We note that the difference of transverse dynamics between the first order phase transition and the cross over transition is consistent in our simulations with the predictions by the hydro+UrQMD approach [92].

For the directed flow v_1 , the softening of the EoS leads to a dramatic effect: negative v_1 values as experimentally observed, for baryons in JAM-1.O.P.T. In stark contrast, the cascade, the crossover, and the mean field simulations predict a positive v_1 -slope. The v_1 value and the sign are very sensitive to the EoS. It is important to study in detail the EoS dependence on the net-baryon density by v_1 in the future. The elliptic flow v_2 develops in time scales compatible with the system size/ c ; hence, v_2 increases between 5 fm/ c and 10 fm/ c . The excitation function of the elliptic flow shown in Fig. 2 demonstrated that JAM/MF yields nearly the same amount of v_2 as the cascade mode, while JAM-1.O.P.T. and JAM- X -over predict larger v_2 values.

The effects of the EoS on the three observables are summarized in Table II: The slope parameter, T_{eff} , is extracted from the fit of the transverse mass m_T distribution of nucleons at mid-rapidity, $|y| < 0.12$, and $m_T - m_0 > 0.5$ GeV, by the exponential function

$$\frac{1}{2\pi m_T} \frac{dN}{dm_T dy} \sim \exp\left(-\frac{m_T}{T_{\text{eff}}}\right). \quad (12)$$

The slope of the directed flow measure $F = dv_1/dy$ is extracted by fitting the rapidity dependence of v_1 by the cubic equation $v_1(y) = Fy + Cy^3$ in the rapidity interval $|y| < 0.8$. One can see the distinct features of the effects of the EoS on the flows. Thus, these calculations demonstrate that the combined analysis of radial, directed and elliptic flows provide the wanted information on the effect of the EoS/the early pressure of the system.

The dependence of the flow on the EoS as computed in the hadronic mean field mode as well as for the different implementations of the potentials are compared in Table II for the

different incompressibility values, $K = 270$ and 370 MeV, as well as for the different assumptions of the potentials; scalar or vector type: Radial flow is barely influenced by the details of the model input, the hadronic EoS dependence is rather small at this beam energy. Vector potentials predict larger v_1 values and smaller v_2 values as compared to the values obtained in the simulations by the scalar potentials. However, note the weak dependence of the different modelings and parameters - this leaves our conclusions unchanged.

The rapidity dependence of v_1 and v_2 is investigated in Fig. 10, which shows the transverse mass distribution at mid-rapidity, $|y| < 0.12$, the rapidity dependence of v_1 and v_2 of the nucleons, for mid-central Au+Au collision at $\sqrt{s_{NN}} = 6.4$ GeV. Note the characteristic predictions for all scenarios, not only in the mid-rapidity region, but also the forward/backward rapidities. The enhancement of v_2 at large rapidities in the mean field simulation is due to the enhancement of the directed flow v_1 at forward/backward rapidities [2, 54].

IV. CONCLUSIONS

The EoS dependence of the excitation function of the elliptic flow of protons and charged particles is investigated within the microscopic JAM transport approach. The conjecture originally made by Sorge [54] has successfully pushed in new directions by explicit simulations which employ different consistent scenarios for both the EoS and the hadronic scattering terms in the high baryon density beam energy region at $\sqrt{s_{NN}} = 3 - 30$ GeV. The measurement of radial and elliptic flows provide information on both, the early and the late pressure. The proof that v_2 is highly sensitive to the EoS is done by explicitly taking into account the effects of both, a first order phase transition (or crossover transition), and the hadronic mean fields. Adding measurements of directed flow shows that the combined analysis of all three flow coefficients, the radial, the directed and the elliptic flows allows now to extract the EoS in different expansion scenarios of the system. Hence, experiments to constrain the EoS are doable and the search for a first order phase transition at high baryon densities will be taken up in the near future.

If the compressed matter does undergo a first order phase transition, then the considerable enhancement of both, radial and elliptic flow, are predicted. Simultaneously, a sudden occurrence of the anti-flow of proton's v_1 , to values of v_1 less than zero, proves to be a unique feature of a first-order phase transition at the highest baryon matter densities. Hadronic degrees of freedom enhance the radial flow, but do not enhance the elliptic flow. Without a first order phase transition, only a positive slope of the directed flow v_1 can be achieved. Moreover, it is possible to distinguish between a first order phase transition and a crossover: A crossover does not enhance the radial flow, enhances the elliptic flow, but yields a *positive* slope of the directed flow. These clear differences do allow experimentally to prove whether a first-order phase transition did occur, using simultaneously the radial, the directed and the elliptic flow values. These independent sensitivities to the EoS constitute a unique way to extract firmly the prop-

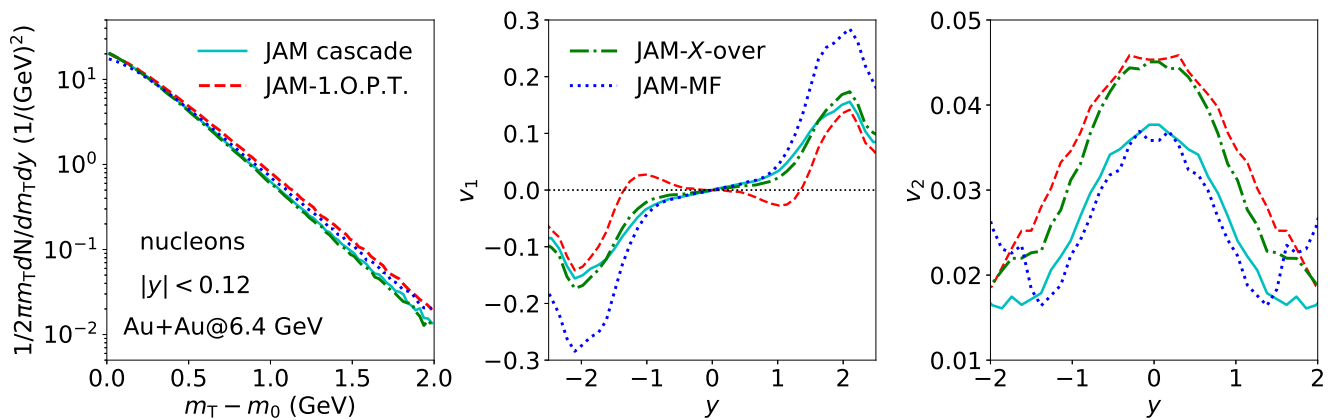


FIG. 10: Transverse mass distribution (left panel), v_1 (middle-panel), and v_2 (right panel) for nucleons in mid-central Au+Au collision at $\sqrt{s_{NN}} = 6.4$ GeV. Solid, dashed, dashed-dotted, and dotted lines show the results from JAM cascade, JAM with first-order phase transition, JAM with crossover EoS, and JAM with hadronic mean field simulations, respectively. Spectator nucleons are excluded in the calculations.

erties of high density baryon matter. In the future, a study of HBT correlations as well as the study of fluctuations of conserved quantities can probe the different expansion dynamics, and search for the conjectured critical point of the EoS. Systematic studies of the centrality dependence, and of various identified particle species's spectrum provide information on heat conduction coefficients, bulk- and shear viscosity values, on top of the EoS dependence of the high density baryon matter created in high energy heavy-ion collisions. The EoS at finite baryon density is still unknown. Therefore, different EoS should be tested experimentally. For example, it will be interesting to use an EoS based on lattice QCD data, e.g. via the PDPL χ RMF [81] and the Quantum van der Waals (QvdW) model [93]. A non-trivial structure is dynamically formed in the chirally symmetric phase by a non-equilibrium time evolution of the chiral σ -field, which is not correlated to the reaction plane, leading to a reduction of elliptic flow in the case of a first order phase transition [82]. As a next step, a non-equilibrium real-time simulation, which treats a phase transition dynamically will be considered.

Future experiments currently planned like, BES II of STAR at RHIC [94], the Compressed Baryonic Matter (CBM) experiment at FAIR [95], MPD at NICA, JINR [96], and a heavy ion experiment at J-PARC (J-PARC-HI) [97] offer opportunities at the most favourable beam energies to explore the high-

est baryon density matter, and to study the phase structure of QCD.

Acknowledgement

H. S. thanks Nu Xu for numerous useful discussions. Y. N. thanks the Frankfurt Institute of Advanced Studies where part of this work was done. This work was supported in part by the Grants-in-Aid for Scientific Research from JSPS (Nos.15K05079, 15K05098, and 17K05448). H. N. has received funding from the European Union's Horizon 2020 research and innovation programme under the Marie Skłodowska-Curie grant agreement no. 655285 and from the Helmholtz International Center for FAIR within the framework of the LOEWE program launched by the State of Hesse. H. St. appreciates the generous endowment of the Judah M. Eisenberg Laureatus professorship. X. Luo is supported in part by the MoST of China 973-Project No.2015CB856901 and NSFC under grant No. 11575069. Computational resources have been provided by the Center for Scientific Computing (CSC) at the J. W. Goethe-University, Frankfurt, and GSI, Darmstadt.

[1] H. Stoecker, J. A. Maruhn and W. Greiner, Phys. Rev. Lett. **44**, 725 (1980).
 [2] H. Stoecker, L. P. Csernai, G. Graebner, G. Buchwald, H. Kruse, R. Y. Cusson, J. A. Maruhn and W. Greiner, Phys. Rev. C **25**, 1873 (1982).
 [3] G. Buchwald, G. Graebner, J. Theis, J. Maruhn, W. Greiner, H. Stoecker, K. A. Frankel and M. Gyulassy, Phys. Rev. C **28**, 2349 (1983).
 [4] H. Stoecker and W. Greiner, Phys. Rept. **137**, 277 (1986).
 [5] P. Danielewicz, R. Lacey and W. G. Lynch, Science **298**, 1592 (2002).

[6] H. Stoecker, Nucl. Phys. A **750**, 121 (2005).
 [7] J. Hofmann, H. Stoecker, U. W. Heinz, W. Scheid and W. Greiner, Phys. Rev. Lett. **36**, 88 (1976).
 [8] C. M. Hung and E. V. Shuryak, Phys. Rev. Lett. **75**, 4003 (1995).
 [9] D. H. Rischke, Y. Pursun, J. A. Maruhn, H. Stoecker and W. Greiner, Heavy Ion Phys. **1**, 309 (1995).
 [10] J. Brachmann, S. Soff, A. Dumitru, H. Stoecker, J. A. Maruhn, W. Greiner, L. V. Bravina and D. H. Rischke, Phys. Rev. C **61**, 024909 (2000).
 [11] Y. B. Ivanov, E. G. Nikonov, W. Noerenberg, A. A. Shanenko

- and V. D. Toneev, *Heavy Ion Phys.* **15**, 117 (2002).
- [12] L. P. Csernai and D. Rohrlich, *Phys. Lett. B* **458**, 454 (1999).
- [13] L. P. Csernai, A. Anderlik, C. Anderlik, V. K. Magas, E. Molnar, A. Nyiri, D. Rohrlich and K. Tamosiunas, *Acta Phys. Hung. A* **22**, 181 (2005).
- [14] J. Brachmann, A. Dumitru, J. A. Maruhn, H. Stoecker, W. Greiner and D. H. Rischke, *Nucl. Phys. A* **619**, 391 (1997).
- [15] L. Adamczyk *et al.* [STAR Collaboration], *Phys. Rev. Lett.* **112**, no. 16, 162301 (2014).
- [16] P. Shanmuganathan [STAR Collaboration], *Nucl. Phys. A* **956**, 260 (2016).
- [17] S. Singha, P. Shanmuganathan and D. Keane, *Adv. High Energy Phys.* **2016**, 2836989 (2016).
- [18] V. P. Konchakovski, W. Cassing, Y. B. Ivanov and V. D. Toneev, *Phys. Rev. C* **90**, no. 1, 014903 (2014).
- [19] J. Steinheimer, J. Auvinen, H. Petersen, M. Bleicher and H. Stoecker, *Phys. Rev. C* **89**, no. 5, 054913 (2014).
- [20] Y. B. Ivanov and A. A. Soldatov, *Phys. Rev. C* **91**, no. 2, 024915 (2015).
- [21] P. Batyuk *et al.*, arXiv:1608.00965 [nucl-th].
- [22] Y. Nara, H. Niemi, A. Ohnishi and H. Stoecker, *Phys. Rev. C* **94**, no. 3, 034906 (2016).
- [23] Y. Nara, H. Niemi, J. Steinheimer and H. Stoecker, *Phys. Lett. B* **769**, 543 (2017).
- [24] H. H. Gutbrod, B. W. Kolb, H. R. Schmidt, A. M. Poskanzer, H. G. Ritter and K. H. Kampert, *Phys. Lett. B* **216**, 267 (1989).
- [25] C. Pinkenburg *et al.* [E895 Collaboration], *Phys. Rev. Lett.* **83**, 1295 (1999).
- [26] A. Andronic *et al.* [FOPI Collaboration], *Phys. Lett. B* **612**, 173 (2005).
- [27] A. Andronic, J. Lukasik, W. Reisdorf and W. Trautmann, *Eur. Phys. J. A* **30**, 31 (2006).
- [28] W. Reisdorf *et al.* [FOPI Collaboration], *Nucl. Phys. A* **876**, 1 (2012).
- [29] P. Danielewicz, R. A. Lacey, P. B. Gossiaux, C. Pinkenburg, P. Chung, J. M. Alexander and R. L. McGrath, *Phys. Rev. Lett.* **81**, 2438 (1998).
- [30] C. Hartnack, J. Aichelin, H. Stoecker and W. Greiner, *Phys. Lett. B* **336**, 131 (1994).
- [31] A. Le Fevre, Y. Leifels, C. Hartnack and J. Aichelin, arXiv:1611.07500 [nucl-th].
- [32] J. J. Molitoris, H. Stoecker, H. A. Gustafsson, J. Cugnon and D. L'Hote, *Phys. Rev. C* **33**, 867 (1986). doi:10.1103/PhysRevC.33.867
- [33] D. E. Kahana, D. Keane, Y. Pang, T. Schlagel and S. Wang, *Phys. Rev. Lett.* **74**, 4404 (1995); D. E. Kahana, Y. Pang and E. V. Shuryak, *Phys. Rev. C* **56**, 481 (1997).
- [34] D. Adamova *et al.* [CERES Collaboration], *Nucl. Phys. A* **698**, 253 (2002).
- [35] K. Filimonov *et al.* [CERES/NA45 Collaboration], *AIP Conf. Proc.* **610**, 556 (2002).
- [36] J. Y. Ollitrault, *Phys. Rev. D* **46**, 229 (1992).
- [37] K. H. Ackermann *et al.* [STAR Collaboration], *Phys. Rev. Lett.* **86**, 402 (2001).
- [38] K. Adcox *et al.* [PHENIX Collaboration], *Phys. Rev. Lett.* **89**, 212301 (2002).
- [39] B. B. Back *et al.* [PHOBOS Collaboration], *Phys. Rev. Lett.* **89**, 222301 (2002).
- [40] B. B. Abelev *et al.* [ALICE Collaboration], *JHEP* **1506**, 190 (2015).
- [41] J. Adam *et al.* [ALICE Collaboration], *Phys. Rev. Lett.* **116**, no. 13, 132302 (2016).
- [42] P. Romatschke and U. Romatschke, *Phys. Rev. Lett.* **99**, 172301 (2007).
- [43] H. Song, S. A. Bass, U. Heinz, T. Hirano and C. Shen, *Phys. Rev. Lett.* **106**, 192301 (2011) Erratum: [*Phys. Rev. Lett.* **109**, 139904 (2012)].
- [44] C. Gale, S. Jeon, B. Schenke, P. Tribedy and R. Venugopalan, *Phys. Rev. Lett.* **110**, no. 1, 012302 (2013).
- [45] H. Niemi, K. J. Eskola and R. Paatelainen, *Phys. Rev. C* **93**, no. 2, 024907 (2016).
- [46] H. Niemi, K. J. Eskola, R. Paatelainen and K. Tuominen, *Phys. Rev. C* **93**, no. 1, 014912 (2016).
- [47] U. Heinz and R. Snellings, *Ann. Rev. Nucl. Part. Sci.* **63**, 123 (2013).
- [48] C. Gale, S. Jeon and B. Schenke, *Int. J. Mod. Phys. A* **28**, 1340011 (2013).
- [49] P. Huovinen, *Int. J. Mod. Phys. E* **22**, 1330029 (2013).
- [50] T. Hirano, P. Huovinen, K. Murase and Y. Nara, *Prog. Part. Nucl. Phys.* **70**, 108 (2013).
- [51] S. Jeon and U. Heinz, *Int. J. Mod. Phys. E* **24**, no. 10, 1530010 (2015).
- [52] A. Jaiswal and V. Roy, *Adv. High Energy Phys.* **2016**, 9623034 (2016).
- [53] H. Stoecker, G. Graebner, J. A. Maruhn and W. Greiner, *Phys. Lett.* **95B**, 192 (1980); H. Stoecker, *Nucl. Phys. A* **418**, 587C (1984).
- [54] H. Sorge, *Phys. Rev. Lett.* **78**, 2309 (1997).
- [55] V. P. Konchakovski, E. L. Bratkovskaya, W. Cassing, V. D. Toneev, S. A. Voloshin and V. Voronyuk, *Phys. Rev. C* **85**, 044922 (2012).
- [56] J. Auvinen and H. Petersen, *Phys. Rev. C* **88**, no. 6, 064908 (2013).
- [57] H. Petersen, Q. Li, X. Zhu and M. Bleicher, *Phys. Rev. C* **74**, 064908 (2006).
- [58] H. Petersen and M. Bleicher, *Phys. Rev. C* **81**, 044906 (2010).
- [59] I. A. Karpenko, P. Huovinen, H. Petersen and M. Bleicher, *Phys. Rev. C* **91**, no. 6, 064901 (2015).
- [60] J. Steinheimer, V. Koch and M. Bleicher, *Phys. Rev. C* **86**, 044903 (2012).
- [61] Y. B. Ivanov and A. A. Soldatov, *Phys. Rev. C* **91**, no. 2, 024914 (2015).
- [62] L. Adamczyk *et al.* [STAR Collaboration], *Phys. Rev. C* **86**, 054908 (2012).
- [63] Y. Nara, N. Otuka, A. Ohnishi, K. Niita and S. Chiba, *Phys. Rev. C* **61**, 024901 (2000).
- [64] M. Isse, A. Ohnishi, N. Otuka, P. K. Sahu and Y. Nara, *Phys. Rev. C* **72**, 064908 (2005).
- [65] H. Sorge, *Phys. Rev. C* **52**, 3291 (1995).
- [66] S. A. Bass *et al.*, *Prog. Part. Nucl. Phys.* **41**, 255 (1998).
- [67] M. Bleicher *et al.*, *J. Phys. G* **25**, 1859 (1999).
- [68] T. Hirano and Y. Nara, *PTEP* **2012**, 01A203 (2012).
- [69] Y. Nara and A. Ohnishi, *Nucl. Phys.* **956**, 284 (2016).
- [70] T. Maruyama, K. Niita, T. Maruyama, S. Chiba, Y. Nakahara and A. Iwamoto, *Prog. Theor. Phys.* **96**, 263 (1996).
- [71] D. Mancusi, K. Niita, T. Maruyama and L. Sihver, *Phys. Rev. C* **79**, 014614 (2009).
- [72] H. Sorge, H. Stoecker and W. Greiner, *Annals Phys.* **192**, 266 (1989).
- [73] T. Ogawa, T. Sato, S. Hashimoto, D. Satoh, S. Tsuda and K. Niita, *Phys. Rev. C* **92**, no. 2, 024614 (2015) Addendum: [*Phys. Rev. C* **92**, no. 2, 029904 (2015)].
- [74] R. Marty and J. Aichelin, *Phys. Rev. C* **87**, no. 3, 034912 (2013).
- [75] J. Xu and C. M. Ko, *Phys. Rev. C* **94**, no. 5, 054909 (2016).
- [76] J. Aichelin, *Phys. Rept.* **202**, 233 (1991); J. Aichelin and H. Stoecker, *Phys. Lett. B* **176**, 14 (1986).
- [77] S. Hama, B. C. Clark, E. D. Cooper, H. S. Sherif and R. L. Mer-

- cer, Phys. Rev. C **41**, 2737 (1990).
- [78] H. Sorge, Phys. Rev. Lett. **82**, 2048 (1999).
- [79] P. Danielewicz and S. Pratt, Phys. Rev. C **53**, 249 (1996).
- [80] J. Sollfrank, P. Huovinen, M. Kataja, P. V. Ruuskanen, M. Prakash and R. Venugopalan, Phys. Rev. C **55**, 392 (1997); P. F. Kolb, J. Sollfrank and U. W. Heinz, Phys. Lett. B **459**, 667 (1999); P. F. Kolb, J. Sollfrank and U. W. Heinz, Phys. Rev. C **62**, 054909 (2000).
- [81] J. Steinheimer, S. Schramm and H. Stoecker, J. Phys. G **38**, 035001 (2011); and Phys. Rev. C **84**, 045208 (2011); P. Rau, J. Steinheimer, S. Schramm and H. Stoecker, Phys. Rev. C **85**, 025204 (2012).
- [82] K. Paech, H. Stoecker and A. Dumitru, Phys. Rev. C **68**, 044907 (2003).
- [83] A. M. Poskanzer and S. A. Voloshin, Phys. Rev. C **58**, 1671 (1998).
- [84] N. Borghini, P. M. Dinh and J. Y. Ollitrault, Phys. Rev. C **63**, 054906 (2001); Phys. Rev. C **64**, 054901 (2001).
- [85] A. Bilandzic, R. Snellings and S. Voloshin, Phys. Rev. C **83**, 044913 (2011).
- [86] C. Adler *et al.* [STAR Collaboration], Phys. Rev. C **66**, 034904 (2002).
- [87] Y. Zhou, K. Xiao, Z. Feng, F. Liu and R. Snellings, Phys. Rev. C **93**, no. 3, 034909 (2016).
- [88] R. Bellwied, S. Borsanyi, Z. Fodor, J. Gunther, S. D. Katz, A. Pasztor, C. Ratti and K. K. Szabo, Nucl. Phys. A **956**, 797 (2016); J. Gunther, R. Bellwied, S. Borsanyi, Z. Fodor, S. D. Katz, A. Pasztor and C. Ratti, EPJ Web Conf. **137**, 07008 (2017).
- [89] K. Niita, S. Chiba, T. Maruyama, T. Maruyama, H. Takada, T. Fukahori, Y. Nakahara and A. Iwamoto, Phys. Rev. C **52**, 2620 (1995).
- [90] J. Chen, X. Luo, F. Liu and Y. Nara, arXiv:1701.00574 [nucl-ex].
- [91] M. Bleicher and H. Stoecker, Phys. Lett. B **526**, 309 (2002).
- [92] H. Petersen, J. Steinheimer, M. Bleicher and H. Stoecker, J. Phys. G **36**, 055104 (2009).
- [93] V. Vovchenko, M. I. Gorenstein and H. Stoecker, Phys. Rev. Lett. **118**, no. 18, 182301 (2017).
- [94] G. Odyniec, EPJ Web Conf. **95**, 03027 (2015).
- [95] T. Ablyazimov *et al.* [CBM Collaboration], Eur. Phys. J. A **53**, no. 3, 60 (2017).
- [96] V. Kekelidze, A. Kovalenko, R. Lednicky, V. Matveev, I. Meshkov, A. Sorin and G. Trubnikov, Nucl. Phys. A **956**, 846 (2016).
- [97] H. Sako *et al.*, Nucl. Phys. A **931**, 1158 (2014); Nucl. Phys. A **956**, 850 (2016).